Constant Directivity Circular-Arc Arrays of Dipole Elements

Richard Taylor[1], Kurtis Manke[1], and D. B. (Don) Keele, Jr.[2]

[1]*Thompson Rivers University, Kamloops BC, Canada*
[2]*DBK Associates and Labs, Bloomington, IN 47408, USA*

Correspondence should be addressed to Richard Taylor (rtaylor@tru.ca)

ABSTRACT

We develop the theory for a broadband constant-beamwidth transducer (CBT) formed by a conformal circular-arc line array of dipole elements. Appropriate amplitude shading of the source distribution leads to a far-field radiation pattern that is constant above a cutoff frequency determined by the prescribed beam width and arc radius. We illustrate the theory with examples, including numerical simulations of magnitude responses, full-sphere radiation patterns and directivity index. Unlike a circular-arc array of monopole elements, a dipole CBT maintains directivity control at low frequency. We give an example of one such array that achieves just 1 dB variation in directivity index over all frequencies.

1 Introduction

Taylor and Keele in [1] developed a comprehensive theory for constant directivity circular-arc (CBT) line arrays. There the arrays were assumed to be formed by a continuous line source of monopole (point source) elements in a circular arc. With appropriate frequency-independent amplitude shading, such an array provides a far-field radiation pattern that is constant above a certain cutoff frequency. The cutoff frequency is determined by the arc radius and the prescribed beam width of the radiation pattern in the plane of the array.

However, it was determined that the array's behavior below the cutoff frequency does not provide any directivity control whatsoever (an observation also corroborated by Keele's earlier simulations and measurements [2, 3]). This is due to the inherent omni-directional behavior of the monopole source elements forming the array. At frequencies significantly lower than the cutoff frequency, where the acoustic wavelength becomes larger than the array dimensions, the radiation pattern approaches the omni-directional characteristic of the source elements (hence a directivity index of 0 dB).

This paper considers a modified form of circular-arc line array that is composed not of monopole point source elements but of directional dipole source elements. In this situation, it is assumed that the orientation of the dipole elements conforms to the circular arc, with each element aiming outwards from the arc's center of curvature, as illustrated later in Fig. 1. The use of dipole elements to form the array provides significant and usable array directivity at low frequencies, which is due to the inherent broadband directivity (4.7 dB directivity index) of the individual dipole elements' radiation pattern.

In other words, this paper builds on the CBT concept by forming a broadband constant-directivity shaded circular-arc source based on dipole sources. The conventional CBT array analyzed in [1] is not broadband because it provides significant directivity only above its cutoff frequency. By contrast, a dipole CBT array provides directivity control at all frequencies.

The aim of this paper is to develop a theory for the dipole CBT concept and explore its possibilities. The paper is structured as follows. In the next section we consider the general theory of radiation from a conformal circular array of dipoles. We derive an expression for the far-field radiation pattern of such an array, in terms of an expansion of the shading function in circular harmonics, and note that a full-circle dipole array cannot produce a usable broadband response. We then use this theory to derive conditions on the amplitude shading that guarantees a frequency-independent beam pattern and constant directivity, which is possible if the radiating portion of the circle is restricted to an arc of 180° or less.

As in our previous paper [1] we explore further two classes of optimized shading functions, adapted to circular-arc arrays, that achieve broadband constant directivity with control over beam width. One is based on a simple cosine function and the other a Chebyshev polynomial. Both shading functions provide excellent beamwidth control.

Finally we present results and simulations that illustrate the application of our theory to the design of both narrow- and wide-beam arrays. We illustrate and compare the performance of two different arrays with magnitude response graphs at different angles and with full-sphere radiation patterns comparing arrays with both monopole and dipole elements.

We further note that a CBT array composed of dipole elements completely eliminates the monopole CBT array

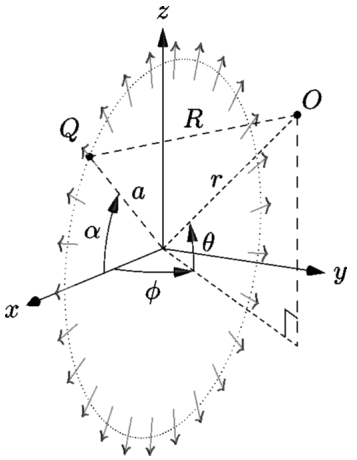

Fig. 1: Geometry of a circular line source of dipoles.

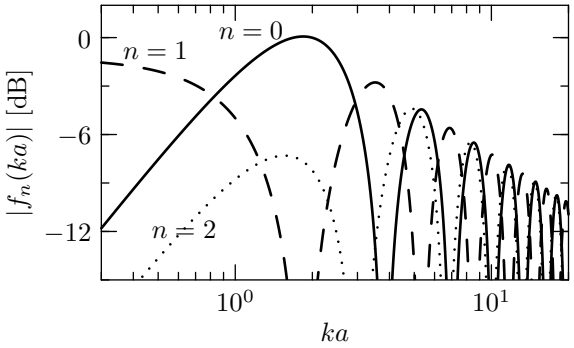

Fig. 2: Mode amplitudes: on-axis far-field pressure, as a function of dimensionless frequency ka, for radiation from a circular array of dipole elements with $\cos(n\theta)$ amplitude shading.

problem of response peaks on either side of the plane of the array, because each dipole element presents a null along this axis. This is a great advantage of the dipole CBT array over the monopole CBT array.

2 Circular Array of Dipoles: Theory

Consider a time-harmonic line source in the form of a circle of radius a, in free space, as shown in Fig. 1. The source elements are taken to be radially-oriented dipoles. (Such an array is said to be *conformal* [4], in that the element orientation changes with the orientation of the array surface.) We adopt a coordinate system in which the circle lies in the xz-plane, with its center at the origin. We take the x-axis ($\theta = \phi = 0$) to be the primary "on-axis" direction of the resulting radiation pattern. We assume the source distribution is iso-phase and continuous, with strength that varies with polar angle α according to a dimensionless and frequency-independent "shading function" $S(\alpha)$ (sometimes also called the amplitude taper).

Referring to Fig. 1, the pressure at O in the far field due to a dipole source at Q, with unit acceleration amplitude, is given (up to a multiplicative constant) by

$$\cos\phi\cos(\theta-\alpha)\cdot\frac{ke^{-ikR}}{R} \tag{1}$$

where k is the wave number [5, p. 312]. Summing such source contributions around the circle gives the total (complex) pressure p via the Rayleigh integral

$$p(r,\theta,\phi) = \int_0^{2\pi} S(\alpha)\cos\phi\cos(\theta-\alpha)\frac{ke^{-ikR}}{R}\cdot a\,d\alpha \tag{2}$$

where

$$\begin{aligned} R &= \sqrt{a^2+r^2-2ar\cos\phi\cos(\theta-\alpha)} \\ &\approx r - a\cos\phi\cos(\theta-\alpha) \qquad (r\gg a). \end{aligned} \tag{3}$$

On making the usual far-field ($r \gg a$) approximations and the change of variables $u = \alpha - \theta$, eq. (2) gives

$$p = \frac{e^{-ikr}}{r}ka\cos\phi\int_0^{2\pi} S(u+\theta)\cos u\, e^{ika\cos\phi\cos u}\,du. \tag{4}$$

We assume the shading function $S(\alpha)$ is even, so it can be expressed as a Fourier cosine series

$$S(\alpha) = \sum_{n=0}^{\infty} a_n\cos(n\alpha) \tag{5}$$

(sometimes called an expansion in circular harmonics). We refer to each term in eq. (5) as a shading mode. On substitution into eq. (4) this gives the far-field radiation pattern

$$p = \frac{e^{-ikr}}{r}ka\cos\phi\sum_{n=0}^{\infty} a_n f_n(ka\cos\phi)\cos(n\theta) \tag{6}$$

with

$$f_n(x) = 2\pi i^n J_n'(x) \tag{7}$$

where J_n is a Bessel function of the first kind [6].

Remarks

- Eq. (6) shows that each circular harmonic shading mode radiates a corresponding far-field pattern of the same polar form. The amplitude of each radiation mode is given by a factor $f_n(ka\cos\phi)$ (the "mode amplitude") that depends only on ϕ and the dimensionless frequency ka.
- Therefore, for a full-circle array of dipoles with single-mode amplitude shading $S(\alpha) = \cos(n\alpha)$, the far-field radiation pattern in any vertical plane through the origin (constant ϕ) is identical to the shading function, at all frequencies.

- For any single shading mode, destructive interference between opposite sides of the array causes a series of nulls in the frequency response, as illustrated in Fig. 2 which plots the mode amplitudes as a function of frequency. Eqs. (6)–(7) show that these nulls occur when $ka\cos\phi$ coincides with an extremum of $J_n(x)$.
- Owing to these frequency response nulls, a full-circle dipole array with single-mode shading cannot produce a usable broadband response. Everywhere in the far field, there are frequencies at which the array radiates zero pressure amplitude.

2.1 Low Frequency Limit

If $a_1 \neq 0$ then using the asymptotic form [6]

$$J_n(x) \approx \frac{1}{n!}\left(\frac{x}{2}\right)^n \qquad (x \ll 1) \tag{8}$$

in eq. (6) gives, to leading order in ka,

$$p \approx a_1 \frac{e^{-ikr}}{r} \pi ika\cos\phi\cos\theta. \tag{9}$$

Thus, at low frequency the array as a whole radiates like a single dipole at the origin, oriented along the x-axis, with strength determined by the coefficient a_1. As Fig. 2 and eq. (6) show, all other shading modes radiate more inefficiently; at sufficiently low frequency their contribution to the far-field radiation is negligible.

3 Conditions for Constant Beam Pattern

Here we derive conditions on the shading function $S(\alpha)$ such that the radiation pattern (4) is independent of frequency. The Bessel functions have the asymptotic form [6]

$$J_n(x) \approx \sqrt{\frac{2}{\pi x}}\cos(x - n\tfrac{\pi}{2} - \tfrac{\pi}{4}) \quad (x \gg n), \tag{10}$$

which on substitution into (7) gives, after some algebra,

$$f_n(x) \approx \sqrt{\frac{8\pi}{x}} \begin{cases} \cos(x+\frac{\pi}{4}) & n \text{ even} \\ i\sin(x+\frac{\pi}{4}) & n \text{ odd.} \end{cases} \tag{11}$$

Thus, provided

$$x \equiv ka\cos\phi \gg n \tag{12}$$

for all non-negligible terms in (6), we obtain

$$p \approx \frac{e^{-ikr}}{r}\sqrt{8\pi x}\left[S_e(\theta)\cos(x+\tfrac{\pi}{4}) + iS_o(\theta)\sin(x+\tfrac{\pi}{4})\right] \tag{13}$$

where

$$\begin{aligned} S_e(\theta) &= \sum_{n \text{ even}} a_n \cos(n\theta), \\ S_o(\theta) &= \sum_{n \text{ odd}} a_n \cos(n\theta). \end{aligned} \tag{14}$$

Eq. (13) gives the pressure magnitude

$$|p| = \frac{\sqrt{8\pi x}}{r}\sqrt{S_e^2(\theta)\cos^2(x+\tfrac{\pi}{4}) + S_o^2(\theta)\sin^2(x+\tfrac{\pi}{4})}. \tag{15}$$

If $|S_e(\theta)| = |S_o(\theta)|$ for all θ then we obtain the far-field pressure

$$|p| = \frac{1}{r}\sqrt{8\pi ka\cos\phi}\,\big|S_o(\theta)\big|. \tag{16}$$

Note that the amplitude of this radiation pattern varies with frequency, but its shape does not.

Thus, the far-field radiation pattern of an amplitude-shaded circular array of dipoles will be independent of frequency, provided the shading function $S(\alpha)$ satisfies the following conditions:

1. $S = S_o + S_e$ with S_o, S_e given by eq. (14) and $|S_o(\alpha)| = |S_e(\alpha)|$ for all α.
2. For all non-negligible coefficients a_n in the cosine series (5) for $S(\alpha)$ we have $ka\cos\phi \gg n$.

These conditions are identical to those discussed in [1] for a circular array of *monopole* elements. Hence, the same conclusions follow. The most important of these are as follows:

- Condition 1 is satisfied if the array is active only on a half-circle on one side of the yz-plane in Fig. 1, i.e. if $S(\alpha) = 0$ for $|\alpha| > \frac{\pi}{2}$. In this case the vertical radiation pattern given by eq. (16) is $|S(\theta)|/2$ and thus is *identical to the shading function* in any vertical plane through the origin (constant ϕ).
- Condition 2 ensures a constant radiation pattern above a cutoff frequency determined by the requirement that $ka\cos\phi \gg n_{\max}$ where $n_{\max}$ is the largest n for which the cosine series coefficient a_n is non-negligible. This condition results in a higher cutoff frequency at greater off-axis angles.
- For frequencies above cutoff, eq. (16) predicts that the far-field pressure decreases at 3 dB/oct with decreasing frequency. Importantly, the response nulls seen for single-mode shading (Fig. 2) are absent.
- The limiting radiation pattern given by eq. (16) is symmetric across the vertical (yz) plane, although the array is not.

4 Optimal Shading

To minimize the cutoff frequency (and thereby achieve a constant radiation pattern over the widest possible band) we require that condition (12) be satisfied down to the lowest frequencies possible. Thus we require a shading function whose Fourier spectrum is concentrated in its lowest-order terms. This criterion is identical to that encountered for circular arrays of monopole elements [1], so that shading functions for that case are equally suitable here.

In [1] we derived circular-arc shading functions of the form

$$S(\theta) = \begin{cases} f(\theta) & |\theta| < \theta_0 \\ 0 & \text{otherwise} \end{cases} \tag{17}$$

where θ_0 is the given half-angle of the circular arc on which the array is active. To concentrate the cosine series coefficients a_n in the lowest-order terms, we found that good candidates for the function $f(\theta)$ are

$$f(\theta) = \cos\left(\frac{\pi}{2} \cdot \frac{\theta}{\theta_0}\right) \tag{18}$$

and

$$f(\theta) = T_N\left(2 \cdot \frac{1+\cos\theta}{1+\cos\theta_0} - 1\right) \tag{19}$$

where T_N is a Chebyshev or Legendre polynomial of degree N. The parameters θ_0 and N determine the arc coverage and the beam width in the plane of the array.

For the special case $\theta_0 = \frac{\pi}{2}$, Jarzynski and Trott [7] showed that the shading function

$$S(\theta) = \tfrac{n}{2n+1}\cos^n\theta + \cos^{n+1}\theta + \tfrac{n+1}{2n+1}\cos^{n+2}\theta \tag{20}$$

is also a good candidate. Here the parameter n controls the beam width.

5 Examples

Here we illustrate our theory by investigating the radiation patterns of circular-arc arrays based on two particular shading functions. One is the degree-6 Chebyshev polynomial shading

$$S(\theta) = \begin{cases} T_6\left(2 \cdot \frac{1+\cos\theta}{1+\cos 52^\circ} - 1\right) & |\theta| \le 52^\circ \\ 0 & |\theta| > 52^\circ \end{cases} \tag{21}$$

which has a -6 dB half-angle of 25° in the plane of the array. The other is the cosine shading

$$S(\theta) = \begin{cases} \cos\left(\frac{9}{7}\theta\right) & |\theta| \le 70^\circ \\ 0 & |\theta| > 70^\circ \end{cases} \tag{22}$$

which has a fairly wide -6 dB half-angle of 47°.

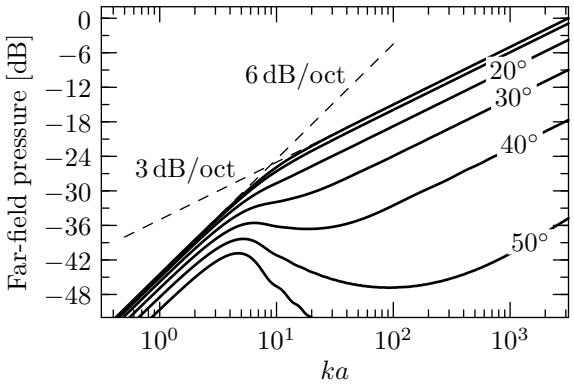

Fig. 3: Far-field magnitude response at various angles θ in the plane of a dipole array with the Chebyshev shading of eq. (21).

Below we present numerical simulations of the radiation patterns that result in these two cases. To facilitate comparison with previous work on CBT arrays of point sources [1, 2, 3, 8, 9], we present results for arrays of both monopole and dipole source elements with identical shading. For the dipole case we have calculated the radiation patterns by numerical quadrature (adaptive Simpson's rule) of the Rayleigh integral in eq. (4). For the monopole case we used eq. (3) of [1].

5.1 Magnitude Response

Fig. 3 shows the raw (unequalized) far-field magnitude responses at various angles θ in the plane of a circular-arc array of dipole elements, with the narrow-beam Chebyshev shading of eq. (21). The responses are plotted against the dimensionless frequency ka (for reference, an array of radius $a = 1$ m has $ka = 1$ at 54 Hz). Fig. 3 confirms several aspects of the theory outlined above:

- There is a clear cutoff frequency (near $ka \approx 10$) above which the radiation pattern transitions from a dipole pattern to a frequency-independent pattern determined by the shading function.
- Below cutoff the level drops at 6 dB/oct toward low frequency, as predicted by eq. (9).
- Above cutoff the level rises at 3 dB/oct, as predicted by eq. (16).
- As expected, the cutoff frequency is higher at greater off-axis angles. On-axis the transition band between low- and high-frequency regimes spans about one octave; at greater off-axis angles the transition band is wider.

In sharp contrast with the single-mode responses of Fig. 2, there are no nulls or even significant ripples in the far-field responses shown in Fig. 3. The array provides a usable broadband response, albeit one that requires significant equalization.

The raw response of a dipole CBT line array is quite different from that of a CBT array of monopole elements, for which the response is 0 dB/oct below cutoff and -3 dB/oct above cutoff [1]. The difference is 6 dB/oct across all frequencies, as might be anticipated in going from monopole to dipole elements. The required equalization curves are correspondingly different: whereas an array of monopole elements requires $+3$ dB/oct equalization above cutoff, the corresponding dipole array requires -3 dB/oct equalization together with a low-frequency dipole equalization of 6 dB/oct.

For both monopole and dipole source elements, Fig. 4 shows far-field magnitude responses normalized to the on-axis ($\theta = 0$) response, for circular-arc arrays with the narrow-beam Chebyshev shading (21). Above $ka \approx 10$ the constant magnitude responses indicate a frequency-independent beam pattern in the plane of the array; this pattern is the same for both monopole and dipole cases, and is determined by the shading function. Fig. 4 also confirms that, as expected, at low frequency the array of monopole elements tends to an omni-directional pattern while the array of dipole elements tends to a dipole pattern (-6 dB at 60° off-axis).

Fig. 5 shows the corresponding responses in the case of the wide-beam cosine shading of eq. (22). The cutoff frequency $ka \approx 3$ is now lower, and there is some ripple (about ± 1 dB) in the transition band. In the case of dipole elements, this ripple is much reduced. In all other respects the response curves in Fig. 5 are exactly as as our theory predicts.

5.2 Full-Sphere Radiation Patterns

To further illustrate the differences between circular-arc arrays of dipole vs. monopole source elements, Fig. 6 shows the full-sphere radiation patterns (polar balloons), normalized on-axis, for arrays with the wide-beam cosine shading of eq. (22). Fig. 6 illustrates several key aspects of the theory developed here and in [1]:

- At low frequency the array of monopole elements exhibits a monopole pattern; the array of dipole elements radiates in a dipole pattern.
- Above cutoff ($ka \approx 5$) both arrays transition to a frequency-independent pattern, which is the product of a vertical pattern determined by the shading function and a horizontal pattern of the form $1/\sqrt{\cos\phi}$ (monopole case) or $\sqrt{\cos\phi}$ (dipole case). At greater off-axis angles the pattern takes longer to settle down.
- The response peaks along the y-axes in the monopole case (due to in-phase superposition of radiation from all source elements) are absent in the dipole case, since in the far field each dipole element presents a null along the y-axes.
- As a result, in the dipole case the radiation pattern is much more consistent between the high- and low-frequency regimes, which leads to much less variation in directivity.

5.3 Directivity Index

The directivity index characterizes the directivity of a radiation pattern $p(r,\theta,\phi)$ in terms of the ratio of the on-axis intensity to that of a point source radiating the same total power [10]. For the coordinate system of Fig. 1 the directivity index is given by

$$\mathrm{DI} = 10\log_{10}\frac{4\pi|p(r,0,0)|^2}{\int_0^{2\pi}\int_{-\pi/2}^{\pi/2}|p(r,\theta,\phi)|^2\cos\phi\,d\phi\,d\theta}. \tag{23}$$

For both our narrow- and wide-beam shading examples, and for both monopole and dipole source elements, Fig. 7 shows the directivity index as a function of dimensionless frequency ka, calculated by numerical quadrature of eq. (23). In the dipole case eq. (4) was used for the radiation pattern; in the monopole case we used equation (3) from [1].

As expected, at low frequency the monopole arrays exhibit 0 dB directivity (monopole radiation) while the dipole arrays have 4.7 dB directivity (dipole radiation). All four examples show increasing directivity in a transition band around the cutoff frequency, above which the directivity becomes constant as determined by the shading function. For both shading functions the dipole-element case comes closer to achieving constant directivity, since there is less loss of directivity at low frequency.

Our cosine-shaded dipole array (Fig. 8, solid line) in particular exhibits remarkably constant directivity (± 0.5 dB) across *all* frequencies. For this array there is very little difference between the radiation patterns above and below cutoff; a slight widening in the horizontal pattern is compensated by a narrowing in the vertical pattern (see Fig. 6).

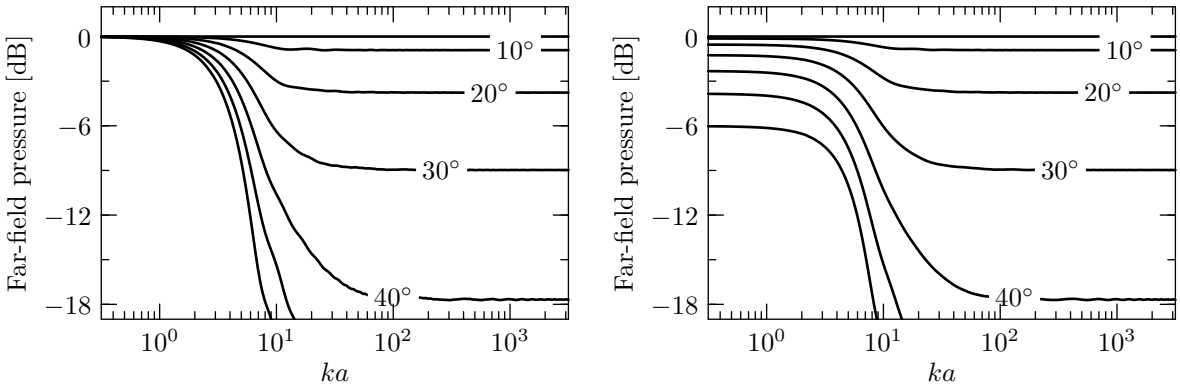

(a) Monopole source elements **(b)** Dipole source elements

Fig. 4: Far-field magnitude responses at various angles θ in the plane of the array, normalized to the on-axis ($\theta = 0$) response, for a circular-arc array of **(a)** a monopole sources, and **(b)** dipole sources. The shading in both cases is the narrow-beam Chebyshev shading of eq. (21).

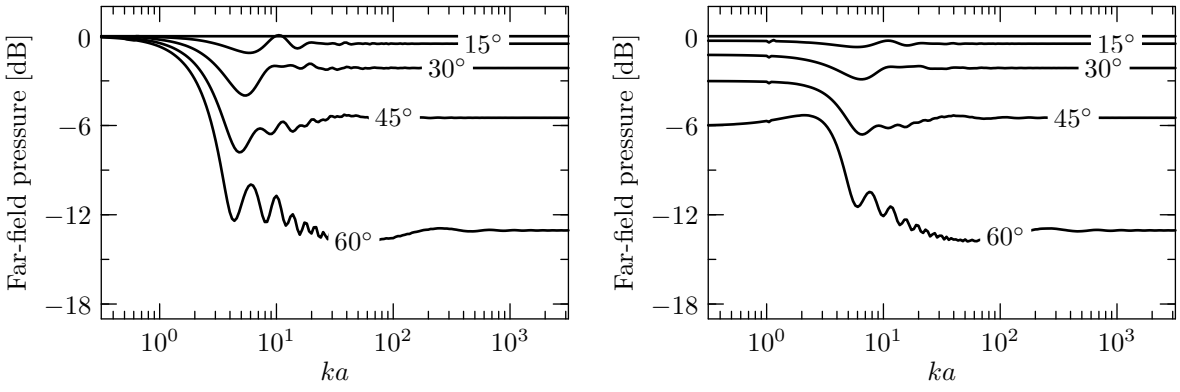

(a) Monopole source elements **(b)** Dipole source elements

Fig. 5: Far-field magnitude responses at various angles θ in the plane of the array, normalized to the on-axis ($\theta = 0$) response, for circular-arc arrays of **(a)** a monopole sources, and **(b)** dipole sources. The shading in both cases is the wide-beam cosine shading of eq. (22).

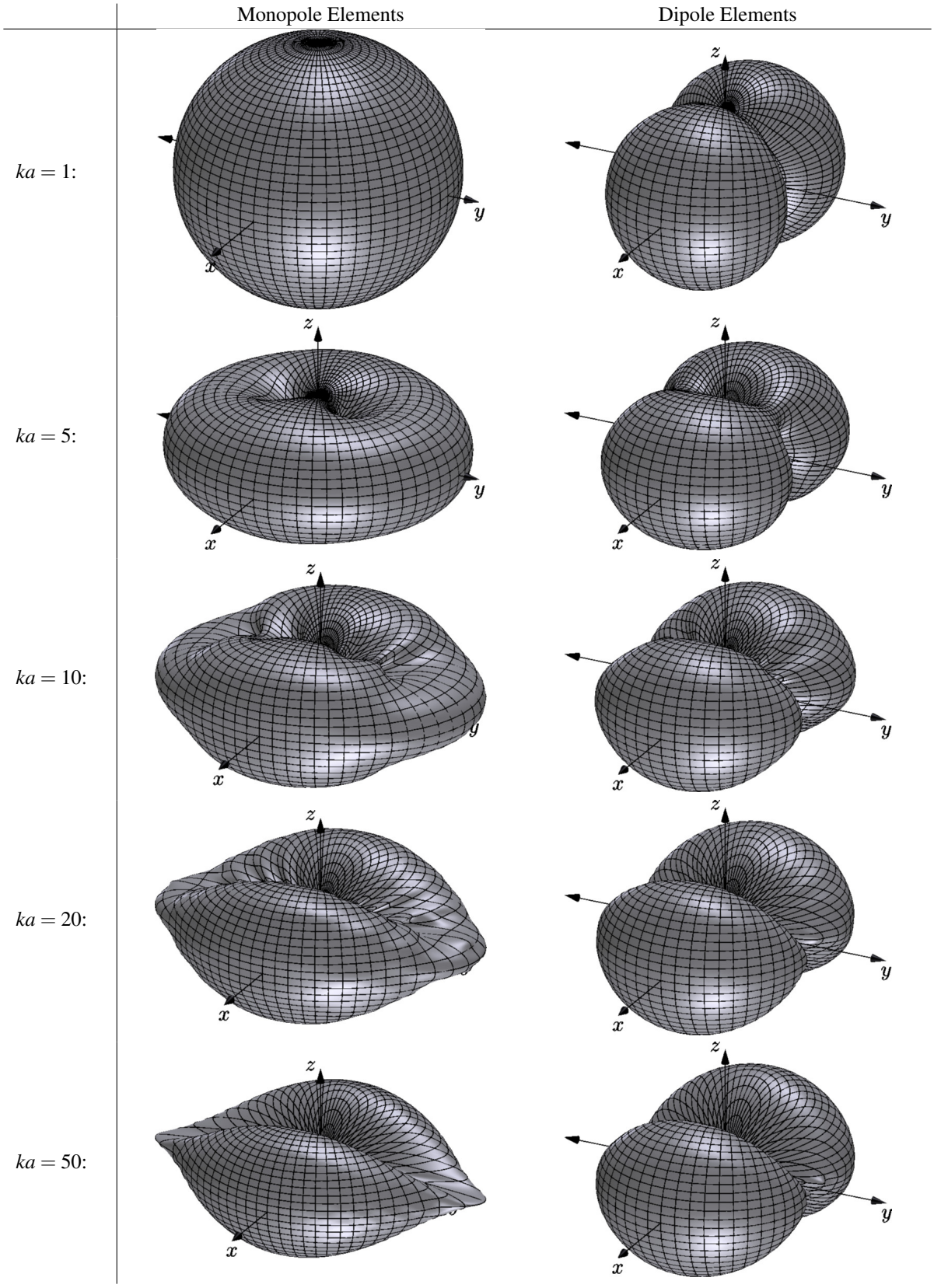

Fig. 6: 3D radiation patterns for circular-arc arrays of both monopole and dipole elements, with the wide-beam cosine shading of eq. (22). The array is oriented as shown in Fig. 1. All plots are normalized on-axis.

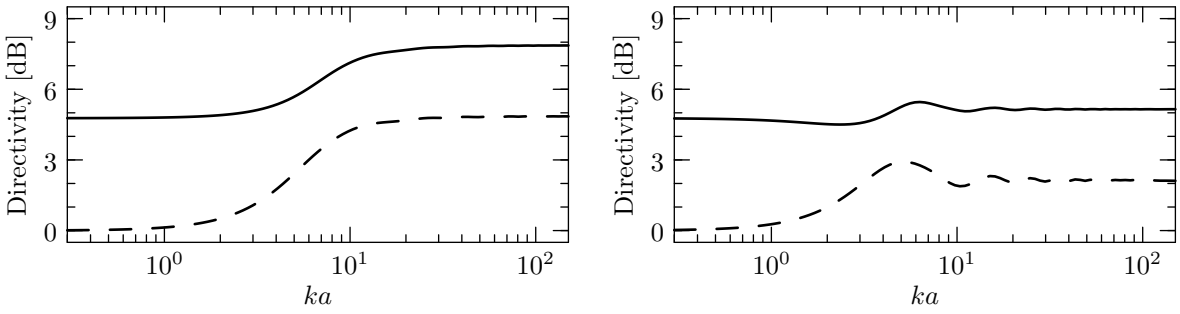

(a) Narrow beam **(b)** Wide beam

Fig. 7: Directivity index vs. frequency for circular-arc arrays with **(a)** the narrow-beam Chebyshev shading of eq. (21), and **(b)** the wide-beam cosine shading of eq. (22). In both cases, results are shown for arrays of both dipole [solid] and monopole [dashed] source elements.

6 Conclusion

We have shown that a constant-directivity source can be formed by a circular-arc array of dipole source elements with frequency-independent amplitude shading. The theory developed here is a natural extension of that presented in [1] for circular arrays of monopole elements, which in turn is an adaptation of the corresponding theory for spherical-cap arrays [7, 11]. An appropriate choice of shading function leads to constant-directivity behavior. Several suitable shading functions appear in the literature, giving the designer access to a variety of beam shapes and widths. The shading function directly determines the radiation pattern in the plane of the array and, together with the arc radius, also determines the cutoff frequency above which a frequency-independent radiation pattern is achieved.

In terms of managing directivity, a dipole CBT array has several advantages over previous CBT designs based on monopole elements [1, 2, 3, 8, 9]. A conventional CBT array becomes omnidirectional below its cutoff frequency (when the array arc is smaller than the acoustic wavelength). This necessitates very large arrays if constant directivity is to be achieved over the whole audio band. By contrast, a CBT array of dipole elements radiates with a dipole pattern (hence with 4.7 dB greater directivity) at low frequency. This makes it possible to achieve broadband constant directivity with small arrays.

At high frequency, a conventional CBT array presents a strong amplitude peak (tens of dB relative to on-axis) along the axis of the circular arc. Although this peak radiates into a small solid angle, and so has little effect on overall directivity, it may nevertheless be undesirable in some applications. A dipole CBT avoids this issue, by placing the dipole null of individual source elements where these peaks would otherwise occur.

Dipole sources are very inefficient radiators, with a response that falls off at 6 dB/oct at low frequency. In a practical implementation this must be compensated by equalization, together with a large radiating area (e.g. in the case of electrostatic panels) and/or large linear displacement (e.g. in the case of conventional piston drivers in an open baffle). This leads to considerable engineering challenges, since large displacement typically incurs high distortion, while to maintain a frequency-independent radiation pattern one requires that the source be acoustically small. CBT dipole arrays address both these issues: being acoustically large by design, a dipole CBT provides a *scalable* way to increase radiating area without compromising the radiation pattern. Indeed, making a CBT array larger actually increases the bandwidth over which constant directivity is achieved.

The low-frequency roll-off of a dipole CBT array must be compensated by equalization if the goal is a flat magnitude response. A naked dipole requires 6 dB/oct equalization at low frequency, which quickly runs into practical limits on driver excursion and signal headroom. However, the raw responses shown in Fig. 3 give an indication of the milder equalization required by a dipole CBT array: above cutoff the slope is only 3 dB/oct. Only below cutoff does the slope increase to 6 dB/oct; with larger arrays the bandwidth of this more demanding regime is reduced. The equalization required for a dipole CBT is quite different from that for an array of monopole elements, which requires only a $+3$ dB/oct boost above cutoff.

A practical device implementing our theory could be formed by a discrete array of conventional drivers, much like that in [3] but with an open baffle. Such a device would necessarily be an approximation of the continuous line source considered here. Several engineering issues arise that are beyond the scope of the

present work. These include effects of discrete sampling of the continuous shading function, spatial aliasing due to finite source spacing, the finite size of both source and baffle, mutual coupling, and the departure of radiating elements from ideal dipole behavior. Much of the relevant theory is presented in [4], and we plan to address these practical issues in subsequent work.

References

[1] Taylor, R. and Keele, Jr., D. B., "Theory of constant directivity circular-arc line arrays," in *Audio Engineering Society Convention 143*, Audio Engineering Society, 2017, manuscript submitted for peer review.

[2] Keele, Jr., D. B., "The full-sphere sound field of constant beamwidth transducer (CBT) loudspeaker line arrays," in *Audio Engineering Society Convention 114*, Audio Engineering Society, 2003.

[3] Keele, Jr., D. B., "Practical implementation of constant beamwidth transducer (CBT) loudspeaker circular-arc line arrays," in *Audio Engineering Society Convention 115*, Audio Engineering Society, 2003.

[4] Josefsson, L. and Persson, P., *Conformal Array Antenna Theory and Design*, Wiley, 2006.

[5] Morse, P. M. and Ingard, K. U., *Theoretical Acoustics*, Princeton University Press, 1987.

[6] DLMF, "*NIST Digital Library of Mathematical Functions*," http://dlmf.nist.gov/, Release 1.0.13, 2016, F. W. J. Olver, A. B. Olde Daalhuis, D. W. Lozier, B. I. Schneider, R. F. Boisvert, C. W. Clark, B. R. Miller and B. V. Saunders, eds.

[7] Jarzynski, J. and Trott, W. J., "Array shading for a broadband constant directivity transducer," *Journal of the Acoustical Society of America*, 64(5), pp. 1266–1269, 1978.

[8] Keele, Jr., D. B., "The application of broadband constant beamwidth transducer (CBT) theory to loudspeaker arrays," in *Audio Engineering Society Convention 109*, Audio Engineering Society, 2000.

[9] Keele, Jr., D. B. and Button, D. J., "Groundplane constant beamwidth transducer (CBT) loudspeaker circular-arc line arrays," in *Audio Engineering Society Convention 119*, Audio Engineering Society, 2005.

[10] Beranek, L. L. and Mellow, T. J., *Acoustics: Sound Fields and Transducers*, Academic Press, 2012.

[11] Rogers, P. H. and Van Buren, A. L., "New approach to a constant beamwidth transducer," *Journal of the Acoustical Society of America*, 64(1), pp. 38–43, 1978.